Eur Biophys J (2003) 32: 655–660
DOI 10.1007/s00249-003-0312-0

BIOPHYSICS LETTER

C. Wilhelm · A. Cebers · J.-C. Bacri · F. Gazeau

Deformation of intracellular endosomes under a magnetic field

Received: 13 February 2003 / Revised: 25 April 2003 / Accepted: 25 April 2003 / Published online: 26 June 2003

Abstract We present a non-invasive method to monitor the membrane tension of intracellular organelles using a magnetic field as an external control parameter. By exploiting the spontaneous endocytosis of anionic colloidal ferromagnetic nanoparticles, we obtain endosomes possessing a superparamagnetic lumen in eukaryotic cells. Initially flaccid, the endosomal membrane undulates because of thermal fluctuations, restricted in zero field by the resting tension and the curvature energy of the membrane. When submitted to a uniform magnetic field, the magnetized endosomes elongate along the field, resulting in the flattening of the entropic membrane undulations. The quantification of the endosome deformation for different magnetic fields allows in situ measurement of the resting tension and the bending stiffness of the membrane enclosing the intracellular organelle.

Keywords Endosome · Magnetic nanoparticle · Membrane deformation · Vesicle

Introduction

Biophysical properties of biological membranes, such as membrane tension or bending stiffness, are critical for many aspects of cellular function, including cell shape, cell motility, surface area regulation, membrane repair, endocytosis, exocytosis and intracellular traffic (Raucher and Sheetz 1999, 2000; Togo et al. 2000; Morris and Homann 2001). The dynamics of intracellular organelles and of transport intermediates includes fission, fusion or tubulation events that may strongly depend upon their membrane properties in relation to the surrounding cytoskeleton (Monck et al. 1990; Sciaky et al. 1997). For living cells, monitoring membrane tension via non-invasive approaches is difficult. This has been successfully achieved for plasma membranes using micropipette aspiration of membrane patches (Evans 1983) or manipulating the membrane via optical or magnetic tweezers acting on a bead attached to the cell surface (Hochmuth et al. 1996; Bausch et al. 1998; Dai et al. 1998). However, up to now, no method exists to constrain, in a mechanically controlled manner, intracellular membranes constitutively organized in vesicles or tubes. Our purpose is to demonstrate the possibility to stress endosomes within a living cell by means of an external magnetic field and in this way to investigate the mechanical properties of their membrane.

C. Wilhelm · J.-C. Bacri · F. Gazeau (✉)
Laboratoire des Milieux Désordonnés et Hétérogènes,
UMR7603, and FR2438 CNRS "Matière et Systèmes Complexes",
Université Pierre et Marie Curie, Tour 13, Case 86,
4 place Jussieu, 75005 Paris, France
E-mail: floga@ccr.jussieu.fr
Tel.: +33-1-44274530
Fax: +33-1-44273854

A. Cebers
Institute of Physics, Latvian Academy of Sciences,
Salaspils-1, 2169 Riga, Latvia

Materials and methods

Methods

Chemically synthesized cobalt ferrite nanoparticles ($CoFe_2O4$) with a mean diameter $d_{np} = 10$ nm were used for the endosomal labeling of HeLa cells. These nanoparticles are coated with negatively charged citrate ligands that ensure their colloidal stability in aqueous suspension through electrostatic repulsions. They are ferrimagnetic single domains bearing a mean magnetic moment of $\mu \approx 1.2 \times 10^{-19}$ A m^2. The magnetic labeling was achieved on the HeLa cell line, grown at 37 °C in 5% CO_2 in Dulbecco's modified Eagle medium supplemented with 10% heat-inactivated fetal calf serum, 50 U/mL penicillin, 40 mg/mL streptomycin and 0.3 mg/mL L-glutamine. The cells were incubated for 1 h at 37 °C with the magnetic nanoparticles at an iron concentration of [Fe] = 10 mM in the extracellular medium (RPMI with 5 mM citrate sodium), followed by 1 h chase in serum-free RPMI. Under these conditions, HeLa cells internalize a mean number of 1.1×10^7 nanoparticles per cell, as quantified by cell magnetophoresis assay (Wilhelm et al. 2002a).

For transmission electron microscopy (TEM) observation, the cells were fixed during 1 h incubation with 2% glutaraldehyde in 0.1 M cacodylate buffer at 4 °C, followed by a postfixation in 1% OsO_4 for 2 h at 4 °C. The cells were then dehydrated in alcohol series and embedded in Epon. Thin sections (70 nm) were examined with a JEOL120CX transmission electron microscope. In order to

visualize the magnetically induced deformation of the endosomes, the cells were exposed to a uniform magnetic field B in the plane of the cell monolayer with an intensity from 0 to 660 mT, during 15 min before and 15 min after glutaraldehyde addition.

Results

A small volume and negative surface charges of the nanoparticles both favor their non-specific adsorption on the plasma membrane, which in turn triggers their internalization within a wide range of cells following the endocytosis pathway (Wilhelm et al. 2002b). Transmission electron micrographs of the magnetically labeled cells show that the dense to electron nanoparticles are confined within organelles like late endosomes of mean diameter $d_{\mathrm{end}} = 0.6$ μm localized throughout the cell cytoplasm (see Fig. 1a). To investigate their magnetic properties, the magnetically labeled intracellular endosomes were purified after cell lysis using a high magnetic field gradient and dispersed in an agarose gel. The magnetization under an applied magnetic field of the endosomal sample was measured using a superconducting quantum interference device (SQUID). The magnetization curve of the purified endosomes shows the behavior of a giant paramagnetic liquid, demonstrating that the nanoparticles are free to rotate in the lumen of the endosome and occupy a volume fraction of 24%. The endosome is not magnetized in zero field, but acquires under a field B a magnetization M_{end} per unit volume, following to a first approximation a Langevin function:

$$M_{\mathrm{end}}(B) = M_{\mathrm{end}}^{(\mathrm{s})}\left(\coth\frac{\mu B}{k_{\mathrm{B}}T} - \frac{k_{\mathrm{B}}T}{\mu B}\right) \quad (1)$$

where $M_{\mathrm{end}}^{(\mathrm{s})} = 55$ kA m^{-1} is the saturation magnetization of the endosome at $B = 5$ T, k_{B} is the Boltzmann constant and T the temperature.

The deformations of the magnetic endosomes can be observed on TEM pictures of cells that are fixed with glutaraldehyde during their exposure to a uniform magnetic field (B varying from 0 to 660 mT) (see Fig. 1). In zero field (Fig. 1a), the endosomes do not appear isotropic, but present protrusions in random directions. Under a magnetic field, the magnetized endosomes (Fig. 1b) conserve a dimpling membrane, but are clearly elongated along the field direction. In order to statistically quantify the magnetically induced deformation, sections of approximately 200 distinct magnetic endosomes for each magnetic field have been analysed, as illustrated in Fig. 2. The endosome outline was first approximated by an ellipse with a major axis $2a$, a minor axis $2b$ and an eccentricity $e = \sqrt{1 - \frac{b^2}{a^2}}$, the major axis being oriented at an angle ϕ with respect to the direction of the magnetic field. Figure 3 shows, for each magnetic field condition (zero field, 20, 45 and 660 mT), four examples of endosomes renormalized to the inner section $\pi(0.3\ \mu\mathrm{m})^2$ and the distribution of the parameters (e,ϕ) measured from the equivalent elliptic contours. In the absence of an external field, the non-zero values of the eccentricities as well as the isotropic orientation of the long axes are the signatures of the thermal fluctuations of the endosome shape. On increasing the magnetic field, the endosome eccentricities augment, while their orientational fluctuations narrow along the direction of the field.

To visualize the averaged shape of the magnetic endosomes, all the normalized endosome section (see Fig. 2), colored with the same grey level, have been superimposed in Fig. 4a. The ''average'' endosome is black in its center and the grey gradation around the outline reflects the amplitude of the shape fluctuations. From all the measured parameters (e,ϕ), we also deduce the outline resulting from averaging all the equivalent elliptic contours, defined in polar coordinates as:

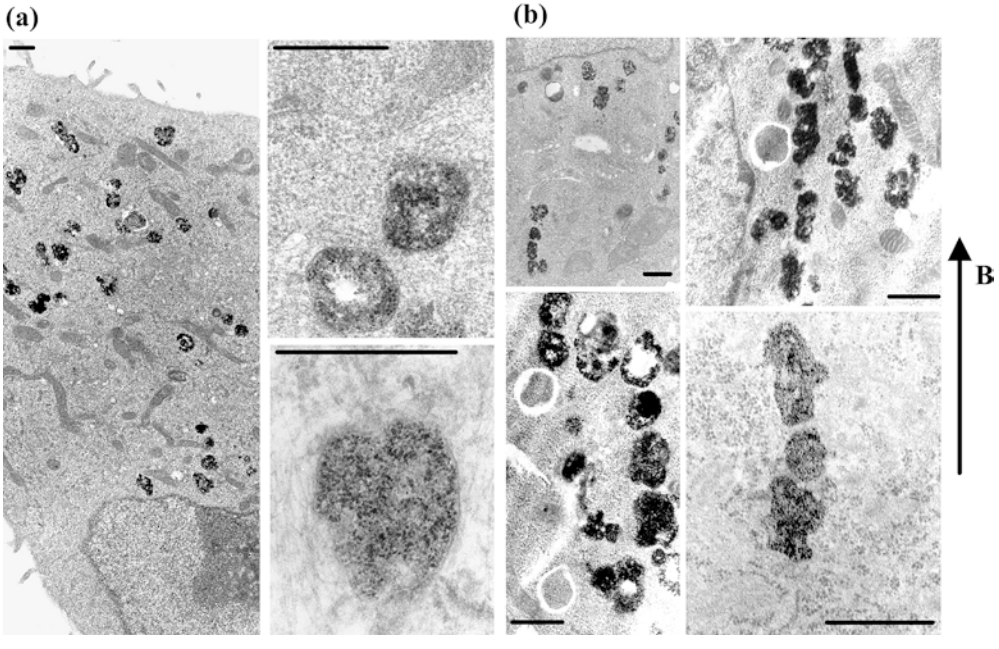

Fig. 1a, b TEM pictures of endosomal magnetic labeling in HeLa cells. The dense to electron nanoparticles are confined within the micrometric membrane bound vesicles (late endosomes). **a** Cells fixed without a magnetic field. **b** Cells fixed during application of a 660 mT magnetic field (15 min before and after glutaraldehyde addition): the magnetic endosomes are elongated and aligned in the direction of the magnetic field. Views at high magnification show the irregular shapes of the endosome external membrane. *Scale bars* are 1 μm

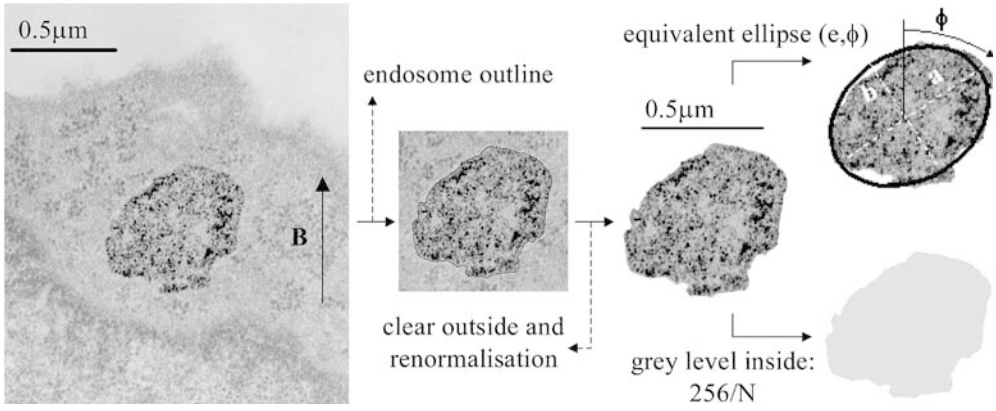

Fig. 2 Image analysis of the magnetic endosome membrane. The endosome outline is drawn, the extraendosomal medium is cleared and the endosome surface is renormalized to $\pi(0.3\ \mu m)^2$. The equivalent ellipse (major axis $2a$, minor axis $2b$) then gives both the eccentricity $e = \sqrt{1 - \frac{b^2}{a^2}}$ and the orientation ϕ with the magnetic field direction for the considered magnetic endosome. Finally, the endosome is filled with a grey level $256/N$, where N is the number of analysed endosomes for each magnetic field B

$$r(\theta) = \frac{1}{N}\sum_{i=1}^{N} r_i(\theta) \tag{2}$$

where:

$$r_i(\theta) = \frac{a_i^2\left[1 + \tan^2(\theta - \phi_i)\right]}{1 + \frac{a_i^2}{b_i^2}\tan^2(\theta - \phi_i)} \tag{3}$$

is the polar coordinate of the ith ellipse. This analytical average of all the equivalent ellipses is represented in Fig. 4a by a white contour superimposed on the fusion of all endosome sections. In zero field, the mean outline is circular. Increasing the magnetic field, the average contour becomes an ellipse elongated along the field direction, with increasing eccentricity. For the intensity of the magnetic field at $B = 20$, 45 and 660 mT, we find respectively the eccentricity of the average contour as $e = 0.38$, 0.56 and 0.68.

Theory

Magnetic endosomes are deformed under a magnetic field because of the competition between the entropic fluctuations of their membrane and the anisotropic magnetic stress induced by the field (Bacri et al. 1996; Ménager et al. 2002). Actually, because the magnetized lumen of the endosome is enclosed in a deformable membrane, its magnetic energy is shape dependent. The endosome deforms in the direction of the magnetic field in order to minimize its total energy by reducing its demagnetizing field. Magnetic surface forces develop on the endosome membrane, due to the magnetic discontinuity at the boundary between the magnetized fluid and the extraendosomal medium. They are normal to the surface and we write, per unit area:

$$\frac{\mu_0}{2}\left(\vec{M}_{\text{end}} \cdot \vec{n}\right)^2 \vec{n} \tag{4}$$

where μ_0 is the vacuum permeability and $\vec{n}$ is the external unit vector. These forces are maximal on the poles of the magnetized endosome, which elongates along the applied field.

The behavior of endosomal membranes can be explained in the framework of the theory which describes the mechanical properties of lipid bilayer vesicles (Helfrich and Servuss 1987; Milner and Safran 1987; Sackmann 1994). Actually, the shape fluctuations of nearly spherical lipid vesicles are understood in terms of a convenient separation of energy scales. While the energy needed to change the area per molecule (and thus to stretch the membrane) is very high, the energy needed to bend the membrane is of the order of the thermal energy, k_BT, and thus governs the strength of thermal membrane undulations. Applying a moderate tension on the membrane, the thermal fluctuations of the vesicles are flattened. If the membrane folds are not resolved by the observation technique, the restriction of the membrane undulations results in an apparent dilation of the visible area of the vesicle. Theoretical and experimental analyses on giant liposomes (Evans and Rawicz 1990; Kummrow and Helfrich 1991; Bacri et al. 1996) show that, in the entropy-driven regime, the tension of the membrane increases exponentially with expansion of the apparent area, the exponential rate or "stiffness" being proportional to the bending rigidity k_c of the membrane. Notwithstanding the difference of spatial scales, the behavior of the average elliptic endosome section (as shown in Fig. 4, the thermal fluctuations of the membrane are hidden in the higher modes of the real contour) is very similar to that of the apparent area of a giant liposome as is observed by optical microscopy with unresolved membrane excess. Thus we are tempted to apply the same formalism. Assuming a large resistance to surface dilation, the real microscopic area $\tilde{A}$ of the endosome is conserved during deformation. In addition, we suppose that exposure to the magnetic field does not entail any changes in the osmotic pressure of the endosome so that its inner volume, V, remains constant. The minimum apparent membrane area, $A_0^{\text{app}} = \pi d_{\text{end}}^2$, in zero field is defined as the area of the equivalent sphere of volume

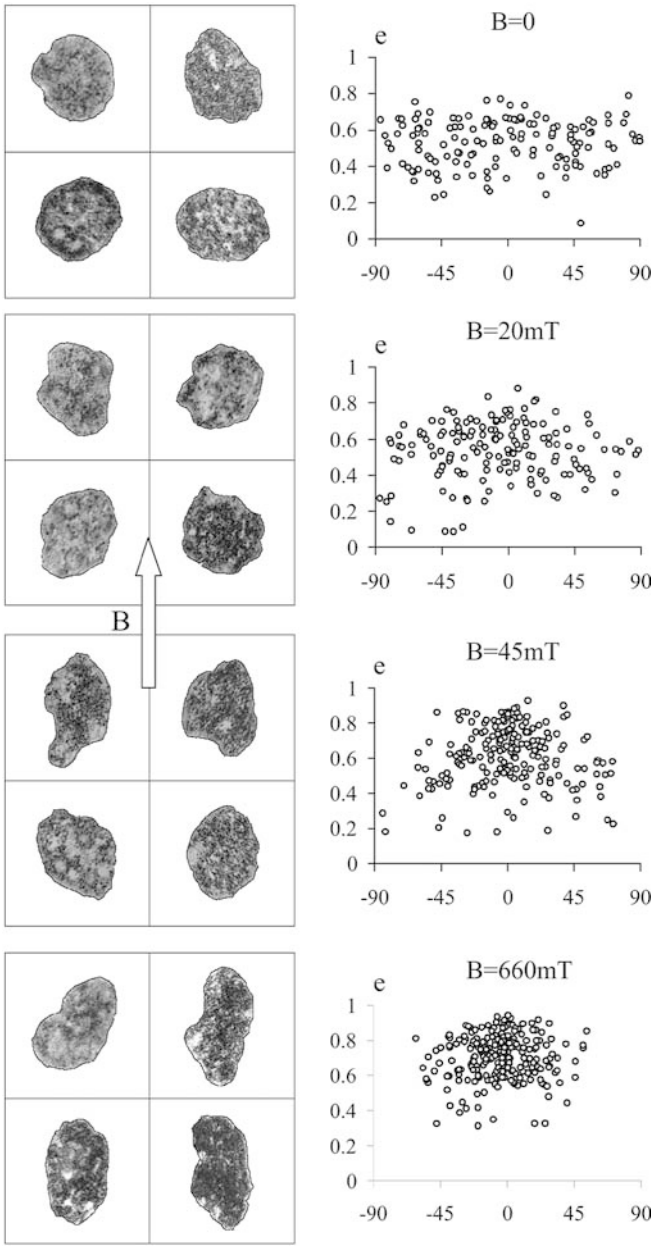

Fig. 3 Statistical analysis of magnetic endosome deformation under a magnetic field. On the *left*, typical endosome outlines (normalized by their inner surface) for each magnetic field B. On the *right*, distributions of the couples (e,ϕ) measured for the N magnetic endosomes analysed for each magnetic field B

$V = \frac{\pi}{6} d_{\mathrm{end}}^3$. Under the magnetic field, the shape of lowest energy for the average endosome, which is consistent with a fixed volume and constrained microscopic area, becomes an axisymmetric prolate ellipsoid with a major axis parallel to the magnetic field direction, an eccentricity e and with a surface area A^{app}. Thus for the increment of the apparent surface area we write:

$$\frac{\Delta A^{\mathrm{app}}}{A_0^{\mathrm{app}}}(e) = \frac{A^{\mathrm{app}} - A_0^{\mathrm{app}}}{A_0^{\mathrm{app}}} = \left\{ \frac{1}{2} \frac{\frac{\arcsin e}{e} + \sqrt{1-e^2}}{(1-e^2)^{1/6}} - 1 \right\} \tag{5}$$

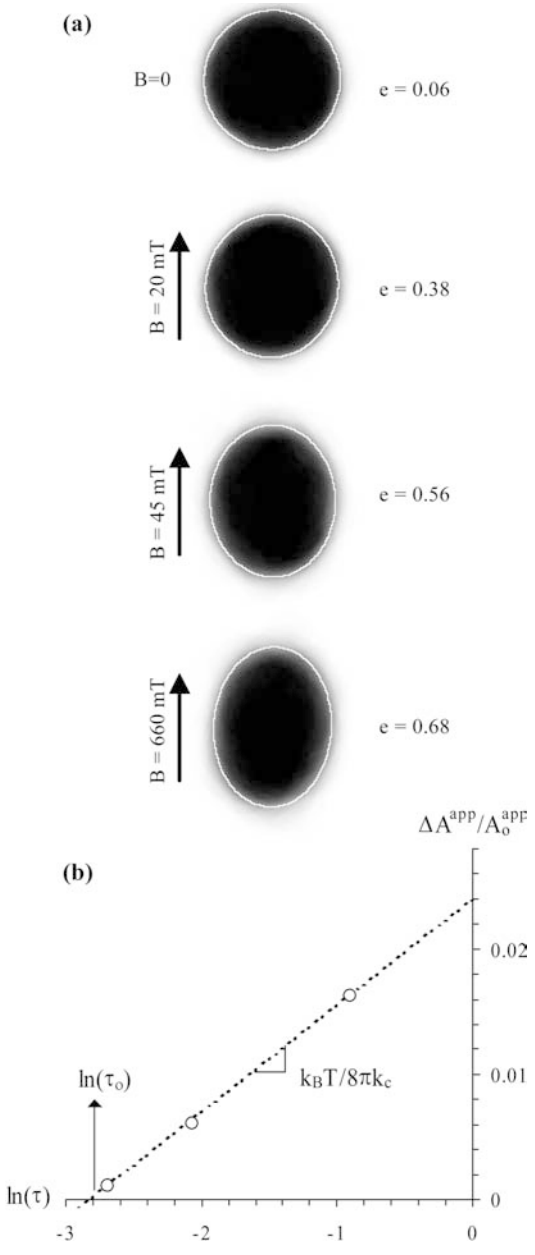

Fig. 4 a Superposition of the N endosome sections filled with a uniform grey level $= 256/N$. The *center* of the obtained surface is *black* (level 256) and the grey gradation reveals the shape fluctuations. The *white line* corresponds to the average contour calculated from all the parameters (e,ϕ) of the equivalent ellipses. The average contour appears to be elliptic, with an eccentricity (indicated on the *right*) increasing with the magnetic field. **b** Dilation of the apparent membrane area $\frac{\Delta A^{\mathrm{app}}}{A_0^{\mathrm{app}}}$ as a function of the logarithm of the membrane tension τ. The linear fit provides the quantitative determination of the bending stiffness, $k_c = 5.2\ k_B T$, and the resting tension, $\tau_0 = 0.06$ mN m^{-1}, for the endomembrane

The magnetic forces at the poles of the ellipsoid increase the tension of the membrane from its initial resting value τ_0 at zero field to its final value $\tau(e)$, that can be deduced from the minimization of the total free energy with respect to the deformation:

$$\tau(e) = f(e) \frac{\mu_0 d_{\mathrm{end}}}{12} (M_{\mathrm{end}}(B_{\mathrm{int}}))^2 \tag{6}$$

where B_{int} is the internal field within the magnetized ellipsoid determined by the implicit equation:

$$B_{\text{int}} = B - \mu_0\{N(e)M_{\text{end}}(B_{\text{int}})\} \tag{7}$$

and where:

$$N(e) = \frac{1-e^2}{2e^3}\left(\ln\frac{1+e}{1-e} - 2e\right) \tag{8}$$

is the demagnetizing factor and:

$$f(e) = 3\left(1-e^2\right)^{2/3}\frac{\frac{3-e^2}{e^6}\ln\frac{1+e}{1-e} - \frac{6}{e^4}}{\frac{3-2e^2}{e^5} - \frac{3-4e^2}{e^3}\frac{\arcsin e}{(1-e^2)^{1/2}}} \tag{9}$$

According to Helfrich and Servuss (1987), the increase of the membrane tension from the resting value τ_0 at zero field to its final value $\tau(e)$ under the field B should result, through the flattening of undulations, in the relative increment of the apparent surface area:

$$\frac{\Delta A^{\text{app}}}{A_0^{\text{app}}} = \frac{k_{\text{B}}T}{8\pi k_{\text{c}}}\ln\frac{\tau(e)}{\tau_0} \tag{10}$$

For the respective intensities of the magnetic field of $B = 20$, 45 and 660 mT, we find the eccentricity of the average contour $e = 0.38$, 0.56 and 0.68 (see Fig. 4), and according to Eqs. (2, 3, 4) the endosome magnetization $M_{\text{end}}(B_{\text{int}}) = 10.6$, 22.7 and 52.9 kA m^{-1}, the relative area dilation $\frac{\Delta A^{\text{app}}}{A_0^{\text{app}}} = 0.11$, 0.61 and 1.63%, and finally the membrane tension $\tau = 0.068$, 0.126 and 0.406 mN m^{-1}. The relative variation of the apparent area $\frac{\Delta A^{\text{app}}}{A_0^{\text{app}}}$ as a function of the napierian logarithm of the tension τ is shown in Fig. 4b. We find a linear dependence over about one decade of the membrane tension. Thus the endosome elongation is correctly described by Eq. (7), yielding $k_{\text{c}} = 5.2 \pm 0.7$ $k_{\text{B}}T$ for the bending rigidity and $\tau_0 = 0.06 \pm 0.01$ mN m^{-1} for the resting tension of the endomembrane under zero field.

Discussion

The description of endosome deformation in terms of the flattening of thermal undulations (Eq. 7) appears to be relevant for endomembrane and submicronic vesicles. It demonstrates that our experimental range of magnetically induced tensions (consistent with the small increment of the apparent membrane area) stays below the crossover from the entropy dominated dynamic regime to the direct elastic compliance of the membrane. It yields the first experimental determination of the mechanical properties of an intracellular organelle membrane: we find $k_{\text{c}} = 5.2 \pm 0.7$ $k_{\text{B}}T$ for the bending rigidity and $\tau_0 = 0.06 \pm 0.01$ mN m^{-1} for the resting tension of the membrane under zero field. For comparison, measurements of the resting tension on plasma membranes have been reported in the order of 0.003 mN m^{-1} for chick neuronal growth cones (Hochmuth et al. 1996) and 0.04 mN m^{-1} for molluscan neurons (Dai et al. 1998). In addition, bending rigidity is found between 10 $k_{\text{B}}T$ for lipid bilayers to 60 $k_{\text{B}}T$ for plasma membranes of various cells. Monck et al. (1990) assumed that exocytotic granule membranes support higher tension than plasma membranes, the tension difference being critical for bringing about exocytotic fusion. Here we show that magnetic late endosomes within HeLa cells appear to be flaccid with a significant resting tension (compared to plasma membrane), but low bending stiffness. A comparable bending stiffness has been measured by flicker spectroscopy for the erythrocyte membrane (Zilker et al. 1992). Such a low bending stiffness may be related to the peculiar protein-lipid composition of endosomal membranes (Kobayashi et al. 2002) that differs from plasma membranes due to its specific biogenesis and fate in the endocytosis pathway. Actually, incorporation of macromolecules into model membranes has been found to reduce the bending stiffness (Häckl et al. 1997). In addition, the mechanical properties of endosomal membranes are here measured in situ, while the endosome suffers various interactions from its local environment. In particular, the underlying anisotropic network of microtubules on which the endosomes are able to travel may affect the endosome shape and apparent rigidity. It was reported that transport of vesicles along microtubules by motor proteins encouraged vesicle elongation (Bananis et al. 2000) and tubulation (Roux et al. 2002). Thus, interactions with the locally anisotropic cytoskeleton through motor proteins may possibly affect the membrane dynamics and the measured parameters. From a functional point of view, the specific membrane dynamics of endosomal compartments should ensure their homotypic and heterotypic fusogenic ability in order to permit membrane and solute exchanges with intravesicular or extravesicular bodies. However, in an attempt to bring biologically relevant information, it should be necessary to measure with the present method the membrane properties of different well-identified intracellular compartments and under modifications of their cytoskeletal environment. So far, it remains remarkable that the minimal description of membrane shape fluctuations at thermodynamic equilibrium successfully accounts for the morphology of intracellular unilamellar organelles. Obviously, biological membranes are submitted to non-equilibrium noise sources due, for instance, to the activity of membrane proteins and superimposed on the thermal noise. It was shown by Manneville et al. (1999) that the biological activity (as proton pumping) induces a magnification of the membrane shape fluctuations, which still can be described by Eq. (7), providing the definition of an effective temperature, higher than the actual one. By this effect, the bending modulus k_{c}, here estimated with the actual temperature, may be underevaluated.

In conclusion, the disposal of magnetic endosomes allows us for the first time to monitor non-invasively

the tension of endomembranes and to deform in vivo intracellular organelles by use of an external control parameter. In addition to this effect on individual organelles, the magnetic endosomes attract each other under a magnetic field through dipole–dipole interactions and align as a chaplet (Valberg 1984) (see Fig. 1). This magnetically induced closeness of organelles, together with their shape elongation, may promote events within living cells such as induced fusion or tubulation, that could potentially interfere with the intracellular membrane trafficking involved in delivery of vesicle contents, targeting and turnover of proteins. It should open new issues for the mechanical manipulations of intracellular organelles.

The observation of endosome deformations induced by a magnetic field also sheds light on the possible mechanisms underlying the geomagnetic sensory system used by various animals for their orientation. Actually, since the discovery of densely packed assemblies of superparamagnetic magnetite particles within the innervated structure of the upper beak skin of the homing pigeon (Holtkamp-Rotzler et al. 1997; Hanzlik et al. 2000), a theoretical model (Shcherbakov and Winklhofer 1999) proposes that such particle assembly with a magnetic field-dependant shape potentially serves as the basis for magnetic field perception. Here we experimentally demonstrate that ferrite nanoparticles dispersed in a liquid and enclosed by a biological membrane located in the cytoplasm are efficient candidates to convert a magnetic stimulus into mechanical strain. However, to have the potential to detect the low intensity of the Earth's magnetic field (0.05 mT), magnetoreceptive cells must bring into play amplification mechanisms of the magnetic stimulus, or possess highly sensitive mechanoreceptive units as actual transducers.

Acknowledgements We thank L. Legrand for the SQUID measurements, S. Neveu for providing us the nanoparticles, B. Dacrossa for her technical assistance in TEM and E. Coudrier for fruitful discussions.

References

Bacri JC, Cabuil V, Cebers A, Menager C, Perzynski R (1996) Flattening of ferro-vesicle undulations under a magnetic field. Europhys Lett 33:235–240

Bananis E, Murray JW, Stockert RJ, Satir P, Wolkoff AW (2000) Microtubule and motor-dependent endocytic vesicle sorting in vitro. J Cell Biol 151:179–186

Bausch AR, Ziemann F, Boulbitch AA, Jacobson K, Sackmann E (1998) Local measurements of viscoelastic parameters of adherent cell surfaces by magnetic bead microrheometry. Biophys J 75:2038–2049

Dai J, Sheetz MP, Wan X, Morris CE (1998) Membrane tension in swelling and shrinking molluscan neurons. J Neurosci 18:6681–6692

Evans EA (1983) Bending elastic modulus of red blood cell membrane derived from buckling instability in micropipet aspiration tests. Biophys J 43:27–30

Evans EA, Rawicz W (1990) Entropy-driven tension and bending elasticity in condensed-fluid membranes. Phys Rev Lett 64:2094–2097

Häckl W, Seifert U, Sackman E (1997) Effect of fully and partially solubilized amphiphiles on bilayer bending stiffness and temperature dependence of the effective tension of giant vesicles. J Phys II (Paris) 7:1141–1157

Hanzlik M, Heunemann C, Holtkamp-Rotzler E, Winklhofer M, Petersen N, Fleissner G (2000) Superparamagnetic magnetite in the upper beak tissue of homing pigeons. Biometals 13:325–331

Helfrich W, Servuss RM (1987) Undulations, steric interaction and cohesion of fluid membranes. Nuovo Cimento 3D:137–151

Hochmuth FM, Shao JY, Dai J, Sheetz MP (1996) Deformation and flow of membrane into tethers extracted from neuronal growth cones. Biophys J 70:358–369

Holtkamp-Rotzler E, Fleissner G, Hanzlik M, Petersen N (1997) The morphological structure of a possible magnetite-based magnetoreceptor in birds. Ann Geophys 15:117

Kobayashi T, Beuchat MH, Chevallier J, Makino A, Mayran N, Escola JM, Lebrand C, Cosson P, Kobayashi T, Gruenberg J (2002) Separation and characterization of late endosomal membrane domains. J Biol Chem 277:32157–32164

Kummrow M, Helfrich W (1991) Deformation of giant lipid vesicles by electric field. Phys Rev A 44:8356–8360

Manneville JB, Bassereau P, Lévy D, Prost J (1999) Activity of transmembrane proteins induces magnification of shape fluctuations of lipid membranes. Phys Rev Lett 82:4356–4359

Ménager C, Meyer M, Cabuil V, Cebers A, Bacri JC, Perzynski R (2002) Magnetic phospholipid tubes connected to magnetoliposomes: pearling instability induced by a magnetic field. Eur Phys J E 7:325–337

Milner ST, Safran SA (1987) Dynamical fluctuations of droplet microemulsions and vesicles. Phys Rev A 36:4371–4379

Monck JR, Alvarez de Toledo G, Fernandez JM (1990) Tension in secretory granule membranes causes extensive membrane transfer through the exocytotic fusion pore. Proc Natl Acad Sci USA 87:7804–7808

Morris CE, Homann U (2001) Cell surface area regulation and membrane tension. J Membr Biol 179:79–102

Raucher D, Sheetz MP (1999) Membrane expansion increases endocytosis rate during mitosis. J Cell Biol 144:497–506

Raucher D, Sheetz MP (2000) Cell spreading and lamellipodial extension rate is regulated by membrane tension. J Cell Biol 148:127–136

Roux A, Cappello G, Cartaud J, Prost J, Goud B, Bassereau P (2002) A minimal system allowing tubulation with molecular motors pulling on giant liposomes. Proc Natl Acad Sci USA 99:5394–5399

Sackmann E (1994) Membrane bending energy concept of vesicle- and cell-shapes and shape-transitions. FEBS Lett 346:3–16

Sciaky N, Presley J, Smith C, Zaal KJ, Cole N, Moreira JE, Terasaki M, Siggia E, Lippincott-Schwartz J (1997) Golgi tubule traffic and the effects of brefeldin A visualized in living cells. J Cell Biol 139:1137–1155

Shcherbakov VP, Winklhofer M (1999) The osmotic magnetometer: a new model for magnetoreceptors in animals. Eur Biophys J 28:380–392

Togo T, Krasieva TB, Steinhardt RA (2000) A decrease in membrane tension precedes successful cell-membrane repair. Mol Biol Cell 11:4339–4346

Valberg PA (1984) Magnetometry of ingested particles in pulmonary macrophages. Science 224:513–516

Wilhelm C, Gazeau F, Bacri JC (2002a) Magnetophoresis and ferromagnetic resonance of magnetically labeled cells. Eur Biophys J 31:118–125

Wilhelm C, Gazeau F, Roger J, Pons JN, Bacri JC (2002b) Interaction of anionic superparamagnetic nanoparticles with cells: kinetic analyses of membrane adsorption and subsequent internalization. Langmuir 18:8148–8155

Zilker A, Ziegler M, Sackmann E (1992) Spectral analysis of erythrocyte flickering in the 0.3–4-μm^{-1} regime by microinterferometry combined with fast image processing. Phys Rev A 46:7998–8001